JOURNAL OF GEOPHYSICAL RESEARCH, VOL. 106, NO. E6, PAGES 12,315–12,323, JUNE 25, 2001

Constraints on the depth of magnetized crust on Mars from impact craters

Francis Nimmo[1]
California Institute of Technology, Pasadena, California

Martha S. Gilmore[2]
Jet Propulsion Laboratory, Pasadena, California

Abstract. Large (diameter greater than ~500 km) Martian impact basins are associated with observed magnetic fields which are statistically distinct from, and smaller than, fields associated with smaller craters. We suggest that this effect arises because impacts cause shock, heating, and excavation, reducing the magnetization of previously magnetized crust. For a simple, uniformly magnetized model the magnetic field at 100 km altitude is reduced by ~50% when a crater-shaped demagnetization zone reaches the base of the magnetized layer. By analogy with terrestrial data, we assume that in Martian craters the zone of demagnetization extends to a depth of 0.04-0.15 crater diameters. On the basis of this assumption, the data suggest that the depth to the base of the magnetized layer on Mars, if uniform, is ~35 km, with lower and upper bounds of 10 and 100 km, respectively. These bounds imply magnetizations of 5-40 A m^{-1} and are consistent with likely Mars geotherms at 4 Gyr B.P.

1. Introduction

One of the most surprising discoveries of Mars Global Surveyor (MGS) was the existence of crustal magnetic anomalies, with magnitudes of up to ~1000 nT as measured at altitudes of ~100 km [*Acuña et al.*, 1999]. The spatial distribution of these anomalies is not random; they are concentrated in the old, southern portion of the planet and in some areas exhibit a quasi-linear appearance [*Connerney et al.*, 1999]. *Acuña et al.* [1999] also observed that large impact basins, such as Hellas and Argyre, did not display large magnetic anomalies. They inferred that the Martian geodynamo must have ceased activity before these basins were formed, around 4 Gyr B.P., although others [e.g., *Schubert et al.*, 2000] dispute this conclusion.

Impact craters are associated with excavation and vaporization of material and heating and impact melt generation [*Melosh*, 1989]. An impact into a magnetized layer would remove some magnetized material and, if the Curie temperature were exceeded, reset the magnetization of some of the remainder. The apparent magnetization might also be reduced by shock demagnetization [*Cisowski and Fuller*, 1978] or the rotation of neighboring blocks during brecciation [*Beals et al.*, 1963]. The likely result of these effects is to reduce the mean magnetization of the area local to the impact and hence produce a magnetic anomaly relative to the surrounding material. Such effects are often seen in terrestrial impact structures [e.g., *Pilkington and Grieve*, 1992]. *Hood* [1987] suggested that lunar magnetic anomalies were caused by antipodal impacts.

In this paper we carry out a survey of the relationship between impact craters and observed magnetic anomalies and use the craters as a crude probe of the probable depth to which magnetization extends. In the next section we describe the data on which our conclusions are based; we then outline our analysis of the data and a simple model which we believe reproduces the features we have observed. Finally, we use the inferred magnetization depth as a bound on ancient Martian geotherms and magnetization strengths.

2. Data

Mars Global Surveyor recorded three components of the global magnetic field at altitudes greater than ~100 km [*Acuña et al.*, 1999]. In this paper we use only the radial component of the magnetic field, hereafter B, which is least affected by ionospheric noise.

[1]Also at Bullard Laboratories, Cambridge, England, United Kingdom.

[2]Now at Department of Earth and Environmental Sciences, Wesleyan University, Middletown, Connecticut.

Paper number 2000JE001325.
0148-0227/01/2000JE001325$09.00

Table 1. Crater Database[a]

Basin	Basin Characteristics			Observations						Reference
	Long., deg	Lat., deg	D, km	N	Alt., km	$\|B\|$, nT	$\sigma_{\|\bar{B}\|}$, nT	$\|B\|_{max}$, nT	P_B	
Hellas	291.0	-43.0	2295	717	123	8.4	7.7	85.0	0.17	1,2,4,5
Utopia	250.0	45.0	1500	421	122	3.0	2.3	13.7	0.01	4,5,6
Argyre	42.0	-49.5	1200	200	118	9.9	6.3	26.0	0.29	1,2,4,5
Isidis	273.0	13.0	1100	133	121	3.9	2.9	12.8	0.07	1,2,4,5
South of Hephaestus	238.4	10.1	1000	96	122	23.3	23.8	110.2	0.54	3,4,5
Prometheus	264.4	-83.6	837	981	94	9.8	12.4	135.5	0.31	2,4,5
Mangala	147.5	-0.9	592	32	134	67.7	88.8	366.3	0.83	3,4,5
overlapping Schiaparelli	346.4	-5.8	560	17	135	20.0	11.4	39.8	0.52	3,4,5
South of Renaudot	296.5	37.5	558	65	112	25.6	19.5	79.4	0.59	3,4,5
West of le Verrier	357.4	-37.9	498	13	170	14.0	7.0	21.7	0.42	3,5
South of Lyot	322.0	41.6	480	48	122	18.2	14.6	71.0	0.50	3,5
Huygens	304.2	-14.0	472	19	122	41.4	33.1	100.2	0.71	2,5
Sirenum	166.4	-43.5	461	45	134	70.5	37.4	211.6	0.84	3,4,5
Schiaparelli	343.3	-2.5	457	19	165	35.8	26.4	80.1	0.07	1,2,5
Ladon	29.4	-18.4	438	29	134	20.7	21.8	71.4	0.53	3,4,5
Cassini	328.2	24.0	435	23	148	37.0	32.8	123.9	0.70	3,4,5

[a]Lat. and long. are latitude and west longitude. N is the number of bins showing a magnetic field which each crater contains; alt. is the mean spacecraft altitude relative to a planetary radius of 3393.5 km; other symbols defined in text. References: 1, *Wilhelms* [1973]; 2, *Wood and Head* [1976]; 3, *Schultz et al.*, [1982]; 4, *Schultz and Frey* [1990]; 5, *Barlow* [1988]; 6, *McGill* [1989].

We used the Mars Quicklook Data Set (M.H. Acuña, personal communication, 2000) which was binned into $1° \times 1°$ (~60 km) bins over altitude increments of 10 km, where the altitude is defined with respect to a spherical Mars of radius 3393.5 km. Thus each location bin might have several values for B, corresponding to measurements taken at different altitudes. In this work, only the value from the lowest altitude bin was used, and we were, in general, concerned with the absolute magnitude of the radial magnetic field $|B|$. The data set was not corrected for spacecraft-induced errors, but these are estimated at ~3 nT [*Acuña et al.*, 1999] and are small compared to most of the signals we are considering. Since the spacecraft altitude was generally $\geq$100 km, a higher spatial resolution (smaller bin size) is unlikely to contain additional information about surface magnetic features.

The crater database was adapted from *Barlow* [1988]; craters larger than 400 km diameter are tabulated in Table 1. There is considerable disagreement about which of the largest topographic depressions may be impact basins. In practice, if the basin appears in the lists of both *Schultz and Frey* [1990] and *Barlow* [1988], we included it. We also included Al Qahira, Huygens, and the structures west of le Verrier and south of Lyot, as there is general agreement that these are impact structures [*Schultz et al.*, 1982; *Wood and Head*, 1976]. The diameter we used was generally that of the principle outer ring [*Schultz and Frey*, 1990]. Craters smaller than 60 km diameter were not considered, as they are unlikely to cause observable magnetic anomalies at $\geq$100 km spacecraft altitude. As we explain below, we assume that most of the observed impact craters postdate the cessation of the inferred Martian geodynamo and are therefore less interested in any older, more degraded features.

Each $1 \times 1°$ location bin for which a measurement of $|B|$ exceeding a lower threshold $|B|_{min}$ (assumed to represent the noise level; see section 3) existed was assigned as being "cratered" or "uncratered" as follows. If the center of the bin was closer to a crater center than one half the tabulated crater diameter D, that bin was assigned as cratered. In general, each crater caused more than one bin to be cratered.

3. Observations

Figure 1a plots the mean value of $|B|$, hereafter $|\bar{B}|$, calculated from all bins assigned to craters within a specified diameter range and using $|B|_{min} = 0$. Figure 1b plots the total number of bins within each diameter range. We have plotted the data for three different choices of diameter range boundaries. The locations of the three sets of boundaries are below Figure 1c. For craters with $D > 300$ km we also plot the mean absolute field associated with each crater and an error bar corresponding to ± 1 standard deviation σ. The main observation (Figure 1a) is that $|\bar{B}|$ is smaller for larger craters. Moreover, there is a relatively sharp reduction in observed magnetic field at around 400-800 km diameter. Tests using $|B|_{min}$=10 nT showed the same effect, except that the value of $|B|$ increased to ~100 nT for craters with diameters $\leq$100 km.

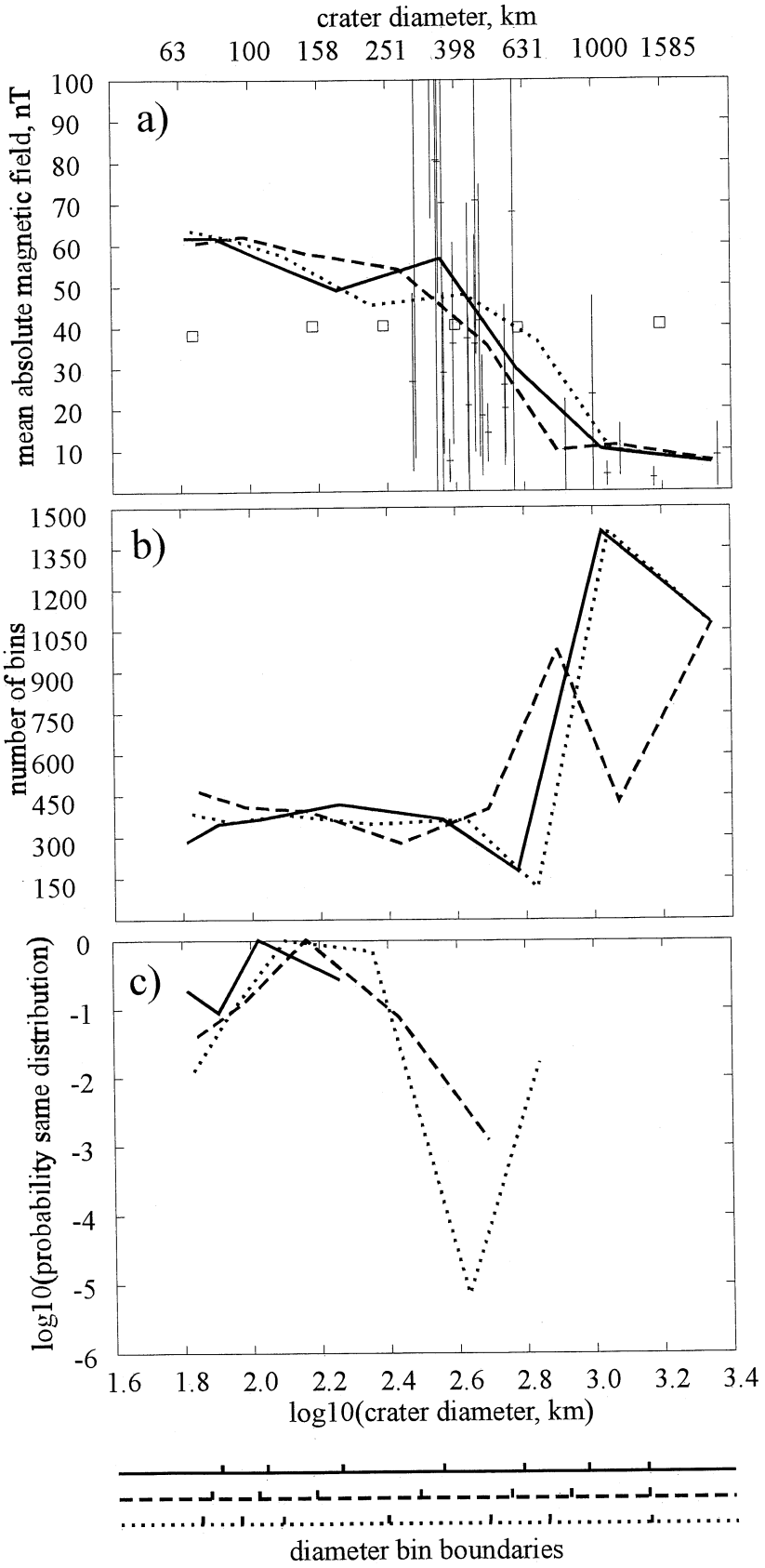

Figure 1. Variation in mean absolute magnetic field with crater diameter. (a) Bold lines are variation in $|\bar{B}|$ with diameter for three different sets of diameter ranges. Thin crosses represent values of $|\bar{B}|$ for individual craters with $D > 300$ km (see Table 1). Vertical lines are $\pm 1\sigma_B$. Squares show mean value of $|\bar{B}|$ from simulations at different crater diameters (see text). Diameter range boundaries are shown below Figure 1c. (b) Bold lines are number of bins for each diameter range. (c) Bold lines are probablities from a Kolmogorov-Smirnoff test that each distribution is drawn from the population for which the probability is 1 (see text). Note the logarithmic scale.

If cratering had no effect on magnetization, one would expect that $|\bar{B}|$ would be independent of crater size. Figure 1a also shows the results of simulations in which 1000 craters of identical sizes are placed randomly on the surface of Mars and $|\bar{B}|$ is calculated. These simulations show that the mean magnetic field which should be observed is ~40 nT, irrespective of diameter. The observations suggest that there is a systematic association between low magnetic field and large craters.

Both the mean and the minimum spacecraft altitude for bins assigned to craters of a given diameter range decrease with increasing diameter, showing that the effect we observe is unlikely to be due to altitude variations. Since the southern hemisphere has a higher proportion of larger craters, and higher magnetic field values, one would expect there to be a positive correlation between crater diameter and magnetic field, which is the reverse of what we observe.

Table 1 shows the mean $|\bar{B}|$ and standard deviation $\sigma_{|B|}$ of $|B|$ and the maximum magnetic field $|B|_{\max}$ observed over craters with $D > 400$ km in the *Barlow* [1988] catalogue. With the exception of Mangala, none of the nine craters larger than 500 km have a value of $|\bar{B}|$ greater than about ~60% of the expected value from simulations. In general, there is an increase in the maximum values of $|\bar{B}|$ and $|B|_{\max}$ as one goes to smaller crater sizes.

The bins in each crater diameter range can be used to obtain the probability distribution function of the observed magnetic field for that size range of crater. In order to test whether large craters have significantly different observed magnetic field distributions from smaller craters, we use the Kolmogorov-Smirnoff test [*Press et al.*, 1992]. Figure 1c shows the log of the probability that the magnetic field distribution for a particular crater size range is the same as that for a specified, intermediate size range. The results show that large craters have observed magnetic field distributions significantly different from those of small and intermediate craters. This result is robust to differences in crater range boundaries.

Finally, for each crater in Table 1 we calculated the probability P_B that a circle of equal size, placed randomly on the planet, would enclose an area showing a value of $|\bar{B}|$ less than or equal to that observed. For the largest craters (diameter $\geq$800 km), P_B is very low but increases at smaller diameters. Such a measure cannot account for the likelihood that preimpact magnetization was not uniform, but at least serves to reemphasize that large craters are associated with systematically small magnetic fields.

Thus the conclusion that large craters (diameter $\geq$400-800 km) have smaller magnetic fields than smaller craters appears to be robust and agrees with the earlier work of *Acuña et al.* [1999].

4. Model

One possible explanation for the above observations is that impact events, owing to removal of preexisting material, shock, and heating, reduce the magnetization of previously magnetized crust. Unfortunately, the depth to which these different effects extend is not clear.

Brecciation and fracturing begins at shock pressures of ~1 GPa [*French*, 1998], and demagnetization has been observed at similar values [*Cisowski and Fuller*, 1978]. *Robertson and Grieve* [1977] estimated shock pressures from exposed rocks at impact sites and used models of shock attenuation to suggest that pressures of ~1 GPa occur at depths comparable to the transient crater radius. On the other hand, *Pohl et al.* [1977] used borehole samples to suggest that peak pressures at 1.2 km depth beneath the 24 km diameter Ries crater may have been <1 GPa. There is thus considerable uncertainty in the depth – peak pressure relationship, which is even greater for larger impact structures. The most direct measurements of the demagnetization zone extent appear to be those of *Scott et al.* [1997]. These authors used a combination of borehole and regional magnetic measurements to conclude that a zone of low magnetization must extend to a few kilometers depth for a crater of diameter 26 km. The depth of demagnetization is thus not well constrained but is probably ~0.1 of the final crater diameter for small terrestrial craters.

The demagnetized zone is likely to be at least as deep as the zone excavated by the impact, which is typically 1/9-1/12 of the transient crater diameter [*Melosh*, 1989]. We will denote the ratio of the demagnetization depth to the final crater diameter by α. For basin-scale impacts the final crater diameter is 1.4-2 times the transient crater diameter [*Melosh*, 1989; *French*, 1998]. Since it is the transient crater diameter which controls the shock attentuation [*Melosh*, 1989], and hence the likely demagnetization depth, α may be reduced for these large impacts. For this study we adopt a value of α of 0.06, but we acknowledge that there are considerable uncertainties in this estimate and discuss this point further in section 5. We also assume that there is no global magnetic field during or after the impact, so that the material affected by impact does not acquire subsequent magnetization. The shape of the demagnetized zone is assumed to be parabolic, and in most cases the surrounding magnetized material extends to the surface.

Figure 2 shows a model of the effect on the observed magnetic field of a demagnetized zone of varying size. Figure 2a shows the geometry of the situation, in which different demagnetized zones are placed in a 20 km thick, 400 km wide layer of material which has a uniform magnetization of 30 A m^{-1}. This slab is flanked by identical slabs with reverse magnetization. For simplicity, the magnetization is directed vertically upward. For $\alpha = 0.06$, demagnetized zones with a diameter >333 km will penetrate the entire magnetized region. We calculate the magnetic field caused by the resulting shape by dividing each stripe into polygons. Uncratered stripes

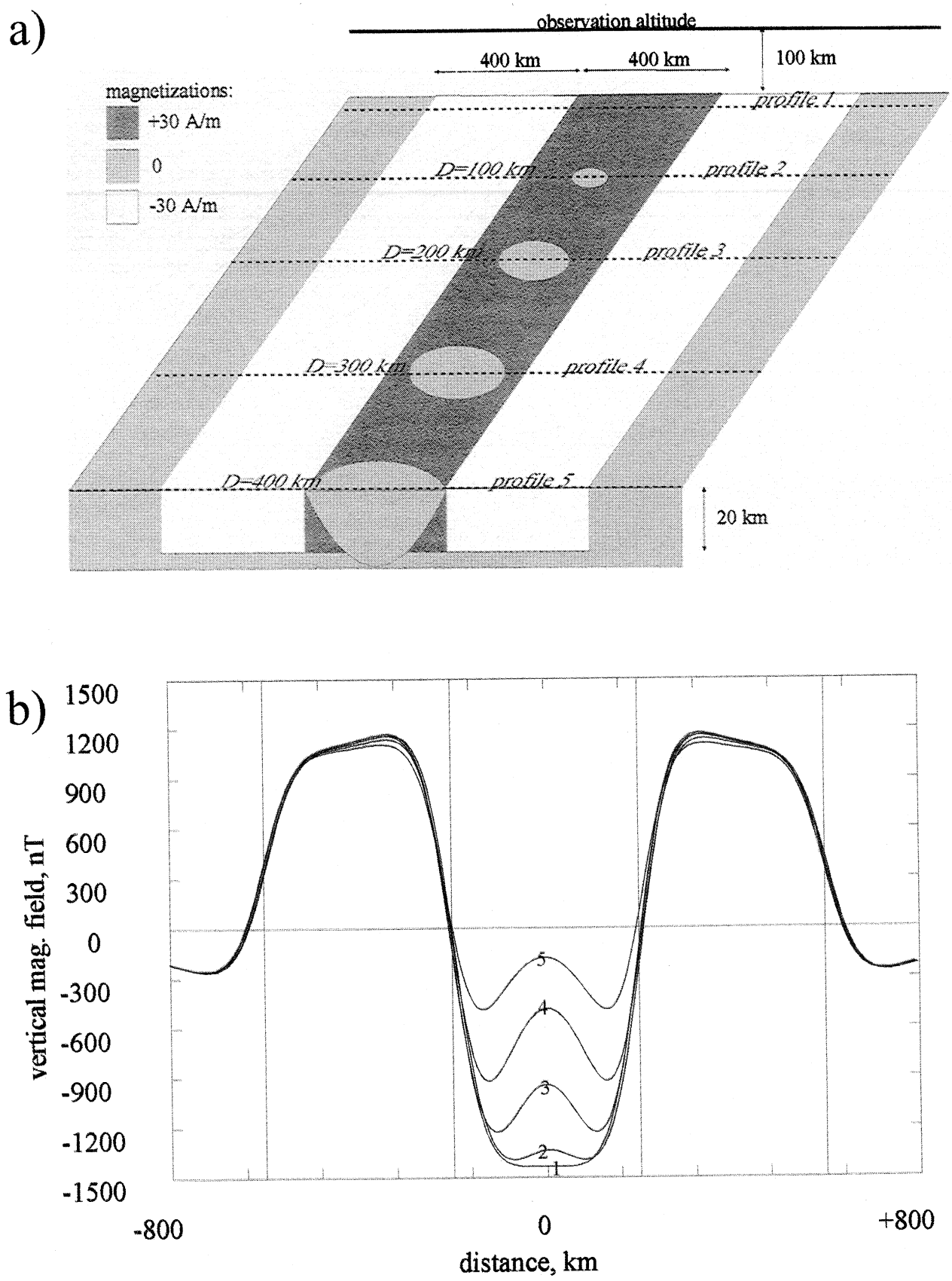

Figure 2. a) Sketch of the model for the effect of impact demagnetization on the observed field, showing location of profiles. D is crater diameter. (b) Results of the calculation of the magnetic field along different profiles. Magnetization is 30 A m^{-1}, directed vertically upward, the magnetized crustal thickness is 20 km, and the altitude of observation is 100 km.

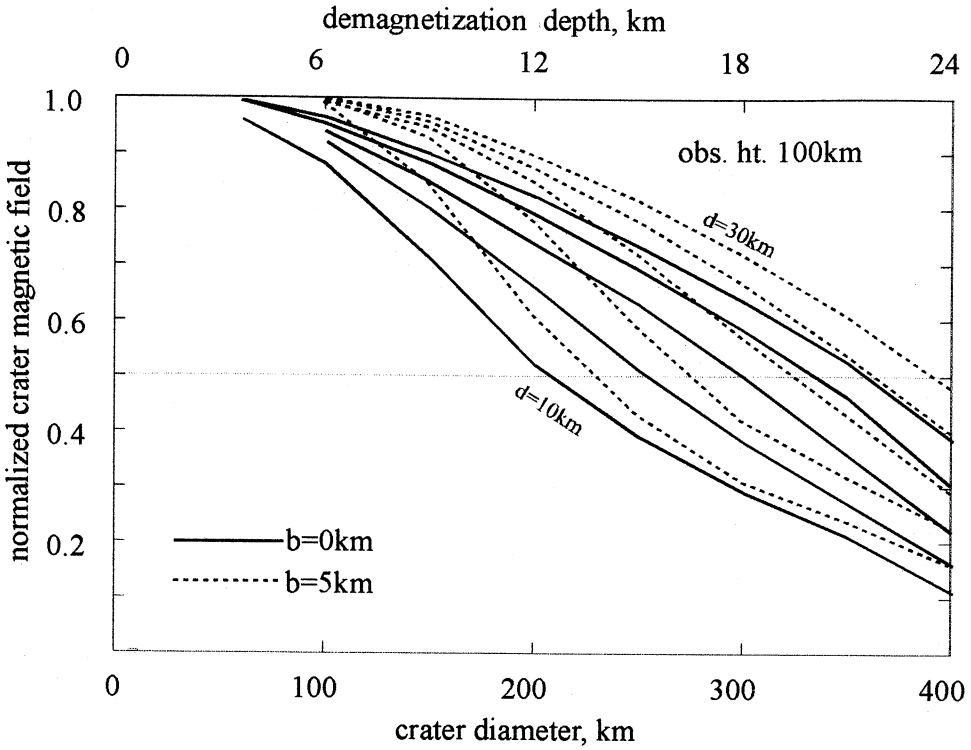

Figure 3. Variation in normalized magnetic field as a function of crater diameter and magnetized layer thickness from calculations as shown in Figure 2b. Observation height is 100 km, and magnetization is 30 A m^{-1}; d is the depth to the base of the magnetized layer, and b is the thickness of the near-surface nonmagnetized layer. Solid lines are for b=0, and dotted lines for b=5 km. Lines are plotted at 5 km intervals in d.

can be represented by six rectangles; for the cratered stripe the demagnetized zone is represented by a series of angled polygons, each of which spans 1 km vertically and 1/100 of the circumference of the zone. The magnetic field due to a series of polygons is then calculated using the method outlined by *Blakely* [1996, Appendix B]. A similar model, for the effect of an impact crater on the magnetic field of the terrestrial seafloor, has been developed by *Ochadlick* [1991].

Figure 2b shows the resulting vertical component of the calculated magnetic field as measured at an altitude of 100 km. As expected, wider craters have a larger effect on the observed magnetic field, both because longer wavelength signals are less attenuated at altitude and because more material has been demagnetized. For a demagnetization zone which just penetrates the entire layer, the mean magnetic field over the crater is about half the value over the undisturbed stripe.

Figure 3 shows the effect of crater demagnetization on the mean magnetic field for different depths to the base of the magnetized layer, d, and observation heights. For cases when the magnetized layer reaches the surface, d is also the thickness of the magnetized layer. Because the magnetization of the layer was kept constant at 30 A m^{-1}, the mean magnetic field over the area of the crater was normalized relative to the mean field over the central 100 km wide portion of the undisturbed central stripe. For an observation height of 100 km the normalizing field varied from 739 nT for d=10 km to 2097 nT for d=30 km.

Figure 3 shows that for craters smaller than the observation altitude, the field is essentially unchanged, as expected. However, larger craters cause the observed field to be reduced. For an observation altitude of 100 km the crater diameter at which the normalized field falls to 0.5 is such that the demagnetization depth approximately equals the magnetized layer thickness. Increasing the altitude to 150 km (not shown) displaces the curves to the right by 10-50 km because small craters have a relatively smaller effect on the observed magnetic field at greater altitudes. Table 1 shows that typical mean observation heights over the large craters are between 100 and 150 km.

The model shown in Figure 2 assumes that the magnetized layer reaches the surface. In fact, the lack of correlation between surface features and magnetic anomalies [*Acuña et al.*, 1999; *Krause and Gilmore*, 2000] suggests that there may be a continuous nonmagnetized layer at the surface. Volcanism postdating the large impacts may account for ~5 km of material [*Greeley and Schneid*, 1991]. The effect of such a layer is simply to increase the effective altitude from which the magnetized layer is observed by an equal amount. If there were a nonmagnetized surface layer of thickness b in existence prior to the large crater formation, it would reduce the amount of material demagnetized by the impact. The

dotted lines in Figure 3 show the effect of a nonmagnetized surface layer with b=5 km. The absolute value of the magnetic field is reduced (because the thickness of magnetized layer is reduced). However, the normalized field is displaced to larger crater diameters because proportionately less magnetized material is demagnetized for a given crater diameter.

We also performed models in which the stripe width was varied from 200 to 600 km and/or the magnetization acquired a nonvertical component. Although the value of the normalizing field changed, we found that a demagnetization depth equal to the layer thickness always resulted in a normalized field $\approx$0.5.

5. Discussion and Conclusions

Figure 3 shows that a decline in the observed magnetic field over a crater as the crater diameter increases may indicate the existence of a magnetized layer of finite thickness. Figure 1a is similar to Figure 3 in that it shows a crater diameter range over which the observed mean magnetic field declines. From Figure 3 this range depends mainly on magnetized layer thickness. For observations at 100 km altitude, similar to the mean altitude over the craters (see Table 1), the excavation depth at which the normalized crater field drops to ~50% of the background value gives the approximate depth to the base of the magnetized layer. The mean magnetic field over small craters from Figure 1a is ~60 nT. The mean field over the craters drops to 30 nT at around D=500-700 km. Thus, for our nominal value of α of 0.06 the implied depth to the base of the magnetized layer is ~30-40 km.

The principal uncertainty in this estimate is in α, the ratio of demagnetization depth to crater diameter. As discussed above, a lower bound on α is probably provided by the depth to which excavation occurs. However, thermal and shock effects may cause demagnetization beneath the base of the excavated zone. For instance, large craters may generate a melt sheet of thickness comparable to αD, which will cool and thermally demagnetize the material below to some fraction of this distance, depending on the Curie temperature. Increasing the demagnetization depth is equivalent to increasing α; higher values of α imply a thicker magnetized layer.

Furthermore, the diameter range over which the observed magnetic field is observed to decrease is also uncertain by at least ±30%. For a case when $\alpha = 0.15$ and the cutoff diameter is 700 km, the depth to the base of the layer is ~100 km. Figure 3 shows that this maximum value is unlikely to be increased by burial effects: for a crater of a given diameter to reduce the observed magnetic field by 50%, the value of d is reduced if there is a surface layer of nonmagnetized material. For a minimum case ($\alpha = 0.04$, D = 250 km) the depth to the base of the layer would be 10 km.

An inherent problem of all magnetic studies is that the results tend to be highly nonunique. In particular, the results we obtain depend on a particularly simple assumption about the preimpact magnetization of the crust. Although we have shown that stripe width and magnetization orientation are unlikely to change the results, we do not incorporate more complex models of spatially varying magnetization, because it is unclear how to do so. In particular, it is almost certainly an oversimplification to assume that the depth to the base of the magnetized layer is constant over the entire planet. However, the paucity of large craters makes regional investigations subject to even greater uncertainties than for the global case. One possible solution would be to model individual profiles [e.g., *Connerney et al.,* 1999].

The bounds on likely magnetized layer thickness, together with the magnitudes of the observed magnetic anomalies, allow constraints to be placed on the mean magnetization. To produce a normalizing field of 1000 nT at an altitude of 100 km, similar to the peak values observed [*Acuña et al.,* 1999], the magnetization of a 400 km wide stripe has to be ~40 A m^{-1} for d=10 km and 5 A m^{-1} for d=100 km. Young (< 2 Ma) terrestrial extrusive mid-ocean ridge basalts have magnetization values of 20-30 A m^{-1} [*Johnson and Salem,* 1994], similar to the maximum values found in subaerial Icelandic basalts [*Kristjansson and Johanesson,* 1999]. These terrestrial values are compatible with those deduced for Mars, especially as Martian basalts are both predicted [*Longhi et al.,* 1992] and observed [*McSween,* 1994] to have a higher iron content.

The most likely magnetic minerals on Mars are magnetite and hematite, which have Curie temperatures of 850 and 950 K, respectively [*Dunlop and Ozdemir,* 1997]. Given a geothermal gradient, these temperatures can be used to obtain an estimate of the maximum depth of the magnetized layer at the time of its formation. The geothermal gradient depends on the distribution of radiogenic materials in the crust and mantle and the contribution of heat from other sources such as secular cooling. For small planets with single-layer mantles such as Mars, the radiogenic heat generation rate is likely to be similar to the surface heat flux [*Nimmo and Stevenson,* 2000], which is not the case for Earth. Estimates of Martian radiogenic element abundances result in heat generation rates per unit mass of 0.8-1.0 times the terrestrial primitive mantle value [*Longhi et al.,* 1992]. At 4 Gyr B.P. these estimates result in a heat flux of 53-67 mW m^{-2} , ignoring any contributions from secular cooling. *Nimmo and Stevenson* [2001] used these estimates, together with assumptions about the degree to which the Martian crust was enriched in radiogenic elements relative to the undepleted mantle, to calculate likely geotherms. Typical terrestrial mid-ocean ridge basalts are enriched in radiogenic elements by a factor p of ~4 relative to undepleted mantle [*Taylor,* 1992]. The maximum value of p is reached when all the radiogenics are extracted into the crust; for mean global crustal thicknesses of 50

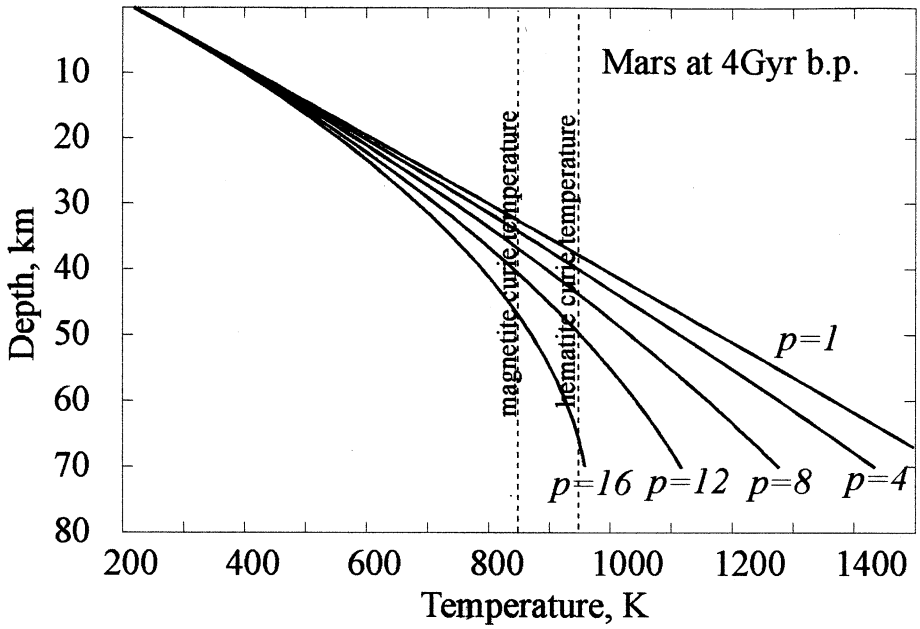

Figure 4. Mars geotherms at 4 Gyr B.P. calculated using method described by *Nimmo and Stevenson,* [2001, equation (13)]. Primitive mantle radiogenic abundances assumed to be 0.9 times the *Sun and McDonough* [1989] terrestrial values. Crustal thickness is 70 km; crustal radiogenic concentrations are p times the primitive mantle concentration. Curie temperatures are from *Dunlop and Ozdemir* [1997]. Core radius is assumed to be 1450 km, and mantle radius is assumed to be 3400 km. Thermal conductivity is 3.2 W m^{-1} K^{-1}, surface temperature is 220 K, and undepleted mantle heat flux is 60 mW m^{-2}.

[*Zuber et al.,* 2000] and 70 km the maximum values of p are 25 and 18, respectively. Greater concentrations of radiogenics in the crust result in lower crustal temperatures. Figure 4 shows representative geotherms for different values of p and a crustal thickness of 70 km. It demonstrates that at 4 Gyr B.P. the maximum likely magnetization depths for magnetite and hematite are 50 and 70 km, respectively. These depths are consistent with the impact-derived upper bound. However, the geothermal constraint would not apply if the magnetized layers were emplaced at the surface and then gradually buried, after cessation of the dynamo, by volcanism, sedimentation, or impact gardening.

Acknowledgments. We are grateful to D. Winterhalter for providing the magnetic data and N. Barlow for her crater database. The comments of the editor, Paul Lucey, and an anonymous reviewer greatly improved this manuscript. F.N. gratefully acknowledges the financial support of Magdalene College, Cambridge, and the California Institute of Technology. M.S.G. was supported by the Jet Propulsion Laboratory, California Institute of Technology, under a contract with the National Aeronautics and Space Administration.

References

Acuña, M. H., et al., Global distribution of crustal magnetizationn discovered by the Mars Global Surveyor MAG/ER experiment, *Science, 284,* 790-793, 1999.

Barlow, N. G., Crater size-frequency distributions and a revised Martian relative chronology, *Icarus, 75,* 285-305, 1988.

Beals, C.S., M.J.S. Innes, and J.A. Rottenburg, Fossil meteorite craters, in *The Moon, Meteorites and Comets,* edited by B.M. Middlehurst, pp. 235-284, Univ. of Chicago Press, Chicago, 1963.

Blakely, R. J., *Potential Theory in Gravity and Magnetic Applications,* 441 pp., Cambridge Univ. Press, New York, 1996.

Cisowski, S.M., and M. Fuller, The effect of shock on the magnetism of terrestrial rocks, *J. Geophys. Res., 83,* 3441-3458, 1978.

Connerney, J.E.P., M.H. Acuña, P.J. Wasilewski, N.F. Ness, H. Rème, C. Mazelle, D. Vignes, R.P. Lin, D.L. Mitchell, and P.A. Cloutier, Magnetic lineations in the ancient crust of Mars, *Science, 284,* 794-798, 1999.

Dunlop, D.J., and O. Ozdemir, *Rock Magnetism: Fundamentals and Frontiers,* 573 pp., Cambridge Univ. Press, New York, 1997.

French, B.M., *Traces of Catastrophe: a Handbook of Shock-Metamorphic Effects in Terrestrial Meteorite Impact Structures,* LPI Contrib. 954, 120 pp., Lunar and Planet. Inst., Houston, Tex., 1998.

Greeley, R., and B.D. Schneid, Magma generation of Mars - Amounts, rates and comparisons with Earth, Moon and Venus, *Science 254,* 996-998, 1991.

Hood, L.L., Magnetic field and remanent magnetization effects of basin-forming impacts on the Moon, *Geophys. Res. Lett., 14,* 844-847, 1987.

Johnson, H. P., and B.L. Salem, Magnetic properties of dikes from the oceanic upper crustal section, *J. Geophys. Res, 99,* 21,733-21,740, 1994.

Krause, M.O., and M.S. Gilmore, The distribution of magnetic sources on Mars as related to surface geology, *Proc. Lunar Planet. Sci. Conf. 31st,* abstract 1603, 2000.

Kristjansson, L., and H. Johanesson, Secular variations and reversals in a composite 2.5 km thick lava section in cen-

tral western Iceland, *Earth Planets Space, 51,* 261-276, 1999.

Longhi, J., E. Knittle, J.R. Holloway, and H. Wanke, The bulk composition, mineralogy and internal structure of Mars, in *Mars*, edited by H.H. Kieffer et al., pp. 184-208, Univ. of Ariz. Press, Tucson, 1992.

McGill, G.E., Buried topography of Utopia Planitia, Mars: Persistence of a giant impact depression, *J. Geophys. Res., 94,* 2753-2759, 1989.

McSween, H.Y. Jr., What have we learned about Mars from SNC meteorites?, *Meteoritics, 29,* 757-779, 1994.

Melosh, H.J., *Impact Cratering: A Geologic Process,* 245 pp., Oxford Univ. Press, New York, 1989.

Nimmo, F., and D.J. Stevenson, The influence of plate tectonics on the thermal evolution and magnetic field of Mars, *J. Geophys. Res., 105,* 11,969-11,980, 2000.

Nimmo, F., and D.J. Stevenson, Estimates of Martian crustal thickness from viscous relaxation of topography, *J. Geophys. Res.*, in press, 2001.

Ochadlick, A.R., Magnetic exploration of ocean crust for craters of impact origin: Model results, *Geophysics, 56,* 1153-1157, 1991.

Pilkington, M., and R.A.F. Grieve, The geophysical signature of terrstrial impact craters, *Rev. Geophys., 30,* 161-181, 1992.

Pohl, J., D. Stoffler, H. Gall, and K. Ernstson, The Ries impact crater, in *Impact and Explosion Cratering*, edited by D.J. Roddy et al., pp. 343-404, Pergamon, New York, 1977.

Press, W.H.,S.A. Teukolsky,W.T. Vetterling, and B.P. Flannery, *Numerical Recipes in Fortran,* 963 pp., Cambridge Univ. Press, New York, 1992.

Robertson, P.B., and R.A.F. Grieve, Shock attenuation at terrestrial impact structures, in *Impact and Explosion Cratering*, edited by D.J. Roddy et al., pp. 687-702, Pergamon, New York, 1977.

Schubert, G., C.T. Russell, and W.B. Moore, Geophysics - Timing of the Martian dynamo, *Nature, 408,* 666-667, 2000.

Schultz, R.A., and H.V. Frey, A new survey of multiring impacts on Mars, *J. Geophys. Res., 95,* 14,175-14,189, 1990.

Schultz, P.H., R.A. Schultz, and J.R. Rogers, The structure and evolution of ancient impact basins on Mars, *J. Geophys. Res., 87,* 9803-9820, 1982.

Scott, R.G., M. Pilkington, and E.I. Tanczyk, Magnetic investigations of the West Hawk, Deep Bay and Clearwater impact structures, Canada, *Meteorit. Planet. Sci., 32,* 293-308, 1997.

Sun, S. S., and W. F. McDonough, Chemical and isotopic systematics of oceanic basalts: Implications for mantle composition and processes, *Geol. Soc. Spec. Pub., 42,* 313-345, 1989.

Taylor, S.R., *Solar System Evolution: A New Perspective,* Cambridge Univ. Press, New York, 1992.

Wilhelms, D.E., Comparison of Martian and lunar multiringed circular basins, *J. Geophys. Res., 78,* 4084-4095, 1973.

Wood, C.A., and J.W. Head, Comparison of impact basins on Mercury, Mars and the Moon, *Proc. Lunar. Sci. Conf. 7th,* 3629-3651, 1976.

Zuber, M.T., et al., Internal structure and early thermal evolution of Mars from Mars Global Surveyor topography and gravity, *Science, 287,* 1788-1793, 2000.

M. Gilmore, Department of Earth and Environmental Sciences, Wesleyan University, 265 Church Street, Middletown, CT 06459. (mgilmore@wesleyan.edu)

F. Nimmo, Bullard Laboratories, Madingley Road, Cambridge, CB3 0EZ, England, UK. (nimmo@esc.cam.ac.uk)

(Received July 14, 2000; revised February 6, 2001; accepted February 26, 2001.)